Draft version September 1, 2025
Typeset using LaTeX **twocolumn** style in AASTeX7.0.1

PAH Emission Spectra and Band Ratios for Arbitrary Radiation Fields with the Single Photon Approximation

Helena M. Richie [1] and Brandon S. Hensley [2]

[1] *University of Pittsburgh, Department of Physics & Astronomy*
[2] *Jet Propulsion Laboratory, California Institute of Technology, 4800 Oak Grove Drive, Pasadena, CA 91109, USA*

ABSTRACT

We present a new method for generating theoretical PAH emission spectra in arbitrary radiation fields. We utilize the single-photon limit for PAH heating and emission to treat individual photon absorptions as independent events. By modeling the absorption and subsequent cooling of PAHs independently, we can construct a set of basis single-photon emission spectra, which can be scaled to an arbitrary radiation field. For grains in the single-photon limit, we find that this method produces strong agreement with existing theoretical emission spectra. We use this model to explore the dependence of PAH band ratios on the radiation field spectrum across grain sizes. We also investigate the limits of this model by quantifying when the single-photon limit breaks down as a function of grain size and radiation field. A Python-based tool and set of basis spectra, which can be used to generate these emission spectra, will be publicly available upon the publication of this paper.

Keywords: Polycyclic aromatic hydrocarbons (1280)

1. INTRODUCTION

Polycyclic aromatic hydrocarbons (PAHs) are believed to be the carriers of the prominent mid-IR emission features frequently observed in galaxies, caused by the absorption and subsequent emission of energy from starlight photons (A. Leger & J. L. Puget 1984; L. J. Allamandola et al. 1985; A. G. G. M. Tielens 2008; A. Li 2020). The relative strengths of these emission features can provide insight into properties of the underlying PAH population, such as the size distribution and ionization fraction. However, observations have shown that the relative strengths of PAH emission features also depend strongly on the spectrum of the illuminating radiation field (D. Baron et al. 2024, 2025), creating a degeneracy in observed band ratios between PAH properties and their environment. Currently available theoretical PAH emission spectra (from B. T. Draine et al. 2021, using the model from B. T. Draine & A. Li 2001) are computed with an assumed radiation field, making it difficult to untangle this degeneracy. To this end, we present a new method for generating theoretical emission spectra for PAHs in arbitrary radiation fields using the single-photon approximation.

Email: helenarichie@pitt.edu

2. THE SINGLE PHOTON APPROXIMATION

The primary source of nanoparticle heating is stochastic photon absorption, predominantly from UV starlight. The energy absorbed from these photons serves to briefly raise the internal temperature of grains, and is eventually re-radiated in the infrared. The rate of photon absorption is determined by the absorption cross-section, $C_{\rm abs}$, which depends on the dust grain size, ionization state, and the photon wavelength. Larger grains, therefore, generally experience a higher rate of photon absorption than smaller grains. In the large grain limit, photon absorptions occur frequently enough that the temperatures of large grains can be approximated as roughly steady-state, since they will typical absorb energy from additional photons before they can cool radiatively down to their ground state. In the diffuse ISM, the steady-state temperature of large grains tends to be ~ 20 K.

Unlike large grains, due to their small $C_{\rm abs}$ and small heat capacities, small ($a \lesssim 50$ Å) grains undergo large temperature fluctuations as they stochastically absorb photons. The absorbed photon energy goes towards raising the grain's vibrational internal energy, which can briefly raise a small grain's temperature from its ground state temperature to hundreds of Kelvin. Across a wide range of radiation fields, the time between photon ab-

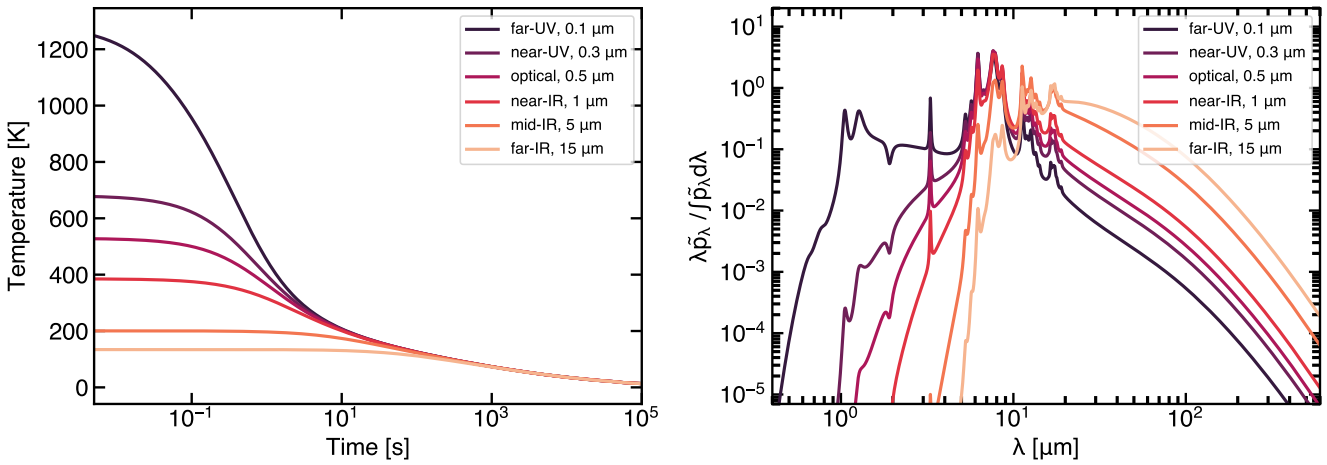

Figure 1. (Left) temperature evolution of a 5 Å ionized PAH as it radiatively cools the energy absorbed from individual photons ranging from far-UV to far-IR wavelengths. (Right) the resulting emission spectra, $\tilde{p}_{\lambda_{\rm em}}(\lambda_{\rm abs})$, which we adopt as our basis spectra.

sorptions for small grains is typically longer than the time it takes for a grain to cool back down to its ground state (B. T. Draine & A. Li 2001). When this condition holds, a grain is in the "single-photon limit", where individual photon absorptions occur independently of one another. Because of this effect, the resulting infrared emission features from these grains (primarily in the $1-10$ μm regime) can be written as a linear combination of these individual photon absorption events.

For a dust grain of a given size and composition, we can determine the spectrum of radiative power per unit wavelength, $\tilde{p}_{\lambda_{em}}(\lambda_{\rm abs})$, corresponding to the absorption of a single photon of wavelength $\lambda_{\rm abs}$. The energy absorbed by the grain is given by

$$E(t=0) = E_{\rm abs} = \frac{hc}{\lambda_{\rm abs}}. \tag{1}$$

In the continuous cooling limit (see B. T. Draine & A. Li 2001), the grain will then cool radiatively according to

$$\frac{dE}{dt} = -\int_{\lambda_{\rm em}} 4\pi B_\lambda(T(t)) C_{\rm abs}(\lambda) d\lambda, \tag{2}$$

where E is the grain's internal vibrational energy and B_λ is the Planck function, which we integrate over all emission wavelengths, $\lambda_{\rm em}$. Given a grain energy model, $E(T)$, one can solve Equation 2 for the grain's temperature evolution, $T(t)$, as it cools to $T \to 0$. At $t = 0$, the grain temperature is given by the corresponding value T such that $E(T) = E_{\rm abs}$. At the ith timestep, the grain energy is given by

$$E_{i+1} = E_{\rm i} + \left(\frac{dE}{dt}\right)_i dt, \tag{3}$$

where $(dE/dT)_i$ is given by Equation 2 with $T(t_i)$ corresponding to $E_i(T)$. Examples of these $T(t)$ are shown in the left panel of Figure 2 for a 5 Å PAH over a range of $\lambda_{\rm abs}$. Then, the total radiative power per unit wavelength for the single-photon absorption is given by

$$\tilde{p}_{\lambda_{\rm em}}(\lambda) = \sum_t 4\pi B_\lambda(T(t)) C_{\rm abs}(\lambda). \tag{4}$$

This $\tilde{p}_{\lambda_{\rm em}}$ can be thought of as a basis spectrum of the corresponding emission from a given grain due to a photon absorption of energy $E_{\rm abs}$. Examples of these basis spectra are shown in Figure 2 for a range of photon wavelengths.

Knowing that $\tilde{p}_{\lambda_{\rm em}}(\lambda_{\rm abs})$ represents the emission spectrum resulting from the absorption of an individual photon, it is possible to determine the full spectrum of a grain due to the many photon absorptions it would experience in a given radiation field, u_λ. We can achieve this by applying a weighting to each $\tilde{p}_{\lambda_{\rm em}}(\lambda_{\rm abs})$ that depends on the strength of the radiation field at each $\lambda_{\rm abs}$. To calculate this weighting, we require that the power absorbed from the radiation field at each $\lambda_{\rm abs}$ is equivalent to the subsequent power radiated over all wavelengths by the grain, i.e. that:

$$\frac{dE}{dt} = \int_{\lambda_{\rm abs}}^{\lambda_{\rm abs}(1+\Delta\lambda)} c u_\lambda(\lambda) C_{\rm abs}(\lambda) d\lambda = \int_{\lambda_{\rm em}} \tilde{p}_{\lambda_{\rm em}}(\lambda_{\rm abs}) d\lambda. \tag{5}$$

Here, we approximate the photon as having a small wavelength range, $[\lambda_{\rm abs}, \lambda_{\rm abs}(1+\Delta\lambda)]$, where $\Delta\lambda$ is a small number (i.e. $\Delta\lambda \lesssim 0.01$), over which it absorbs energy from the radiation field. The radiative power of a grain at each wavelength is then given by

$$p_{\lambda_{\rm em}}(\lambda_{\rm abs}) = \frac{\int_{\lambda_{\rm abs}}^{\lambda_{\rm abs}(1+\Delta\lambda)} cu_\lambda(\lambda) C_{\rm abs}(\lambda) d\lambda}{\int_{\lambda_{\rm em}} \tilde{p}_{\lambda_{\rm em}}(\lambda_{\rm abs}) d\lambda} \tilde{p}_{\lambda_{em}}(\lambda_{\rm abs}). \tag{6}$$

Given a set of basis spectra that spans the entire wavelength range over which a photon absorption could occur, the sum of these $p_{\lambda_{\rm em}}(\lambda_{\rm abs})$ over all $\lambda_{\rm abs}$, i.e.,

$$p_{\lambda_{\rm em}} = \sum_{\lambda_{\rm abs}} p_{\lambda_{\rm em}}(\lambda_{\rm abs}) \tag{7}$$

will be equivalent to the full emission spectrum provided the grain is in the single-photon limit.

3. PAH MODEL

We assume that PAH molecules have a density of 2.0 g cm^{-3} and are composed of $N_{\rm C}$ carbon atoms and $N_{\rm H}$ hydrogen atoms. For a PAH molecule with an effective radius of a, the PAH will contain

$$N_{\rm C} = 418 \left(\frac{a}{10\ \text{Å}}\right)^3 \tag{8}$$

carbon atoms with $N_{\rm C}$ rounded to the nearest integer. The number of hydrogen atoms is defined as

$$N_{\rm H} = \begin{cases} 0.5N_{\rm C} + 0.5 & \text{for } N_{\rm C} \leq 25, \\ 2.5\sqrt{N_{\rm C}} + 0.5 & \text{for } 25 < N_{\rm C} \leq 100, \\ 0.25N_{\rm C} + 0.5 & \text{for } N_{\rm C} > 100, \end{cases} \tag{9}$$

also rounded to the nearest integer.

The internal energy of a PAH molecule can be approximated as the sum of the energy contributions from its individual vibrational degrees of freedom. For a PAH molecule with $N_{\rm C}$ carbon atoms and $N_{\rm H}$ hydrogen atoms, the molecule will have $N_{m,\rm tot} = 3(N_{\rm H} + N_{\rm C} - 2)$ vibrational mode energies resulting from C–C and C–H in-plane and out-of-plane bending and C–H stretching. We adopt the method described in B. T. Draine & A. Li (2001) for modeling the energies of these modes, which we briefly outline here. The model approximates the modes as harmonic oscillators with fundamental frequency ω_j, which allows us to write the expectation value for the energy as a function of temperature,

$$E(T) = \sum_{j=1}^{N_{m,\rm tot}} \frac{\hbar\omega_j}{\exp(\hbar\omega_j/kT) - 1}, \tag{10}$$

assuming the system is in thermal equilibrium.

$$\hbar\omega_j = k\Theta \left[\frac{1-\beta}{N_m}(j - \delta_j) + \beta\right]^{1/2}. \tag{11}$$

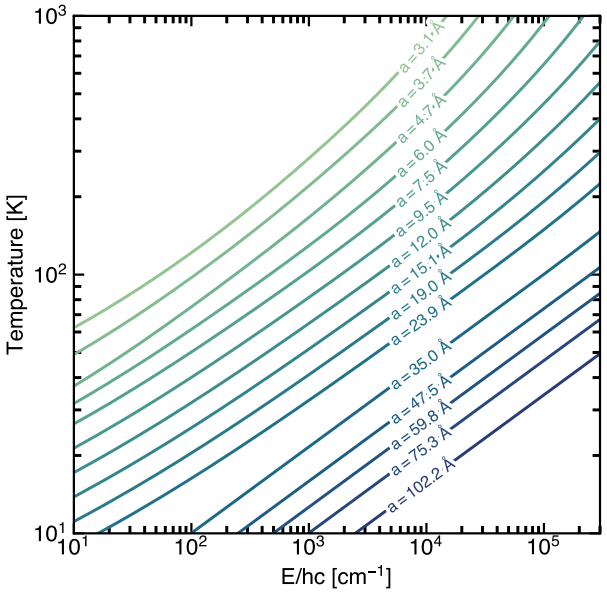

Figure 2. The energy–temperature relation of our PAH model. For $a \leq 26.0$ Å, Equation 10 is used to determine the energy contributions from all PAH vibrational modes. For $a > 26.0$ Å, we replace the energy contributions from C–C modes with the continuum Debye model, Equation 15.

Here, δ_j adjusts the second and third mode frequencies to align with the observed frequencies of coronene,

$$\delta_j = \begin{cases} \frac{1}{2} & \text{for } j \neq 2 \text{ or } 3, \\ 1 & \text{for } j = 2 \text{ or } j = 3 \end{cases} \tag{12}$$

and β describes the shape of the molecule,

$$\beta = \begin{cases} 0 & \text{for } N_{\rm C} \leq 54, \\ \frac{1}{2N_m - 1}\left(\frac{N_{\rm C}-54}{52}\right) & \text{for } 54 < N_{\rm C} \leq 102, \\ \frac{1}{2N_m - 1}\left[\frac{N_{\rm C}-2}{52}\left(\frac{102}{N_{\rm C}}\right)^{2/3} - 1\right] & \text{for } N_{\rm C} > 102 \end{cases} \tag{13}$$

where $N_{\rm C} \leq 54$ is the planar case and $N_{\rm C} > 102$ is the spherical case. The number of modes for C–C in-plane bending is $N_m = N_{\rm C} - 2$ and $N_m = 2(N_{\rm C} - 2)$ for out-of-plane bending.

The C–H vibrational frequencies are taken to be

$$\hbar\omega_j = k\Theta, \tag{14}$$

where $\Theta_{\rm op,CH} = 1257$ K, $\Theta_{\rm ip,CH} = 1670$ K, and $\Theta_{\rm str,CH} = 4360$ K, corresponding to frequencies of 11 μm^{-1}, 8.6 μm^{-1}, and 3.3 μm^{-1}, respectively. For each C–H mode, there will be $N_m = N_{\rm H}$ contributions to Equation 10.

For large PAHs, the number of modes can become quite large. Therefore, we use the method described above to calculate $E(T)$ for grains of size $N_{\rm C} \leq 7360$. For grains of larger sizes, we replace the contributions from the C–C modes in Equation 10 with the continuum Debye model:

$$E_{\rm PAH}^{\rm C-C} = 2\left(N_{\rm C}-2\right)\left[k\Theta_{\rm op}\left(\frac{T}{\Theta_{\rm op}}\right)^3\int_0^{\Theta_{\rm op}/T}\frac{u^2du}{e^u-1}\right.$$
$$\left.+2k\Theta_{\rm ip}\left(\frac{T}{\Theta_{\rm ip}}\right)^3\int_0^{\Theta_{\rm ip}/T}\frac{u^2du}{e^u-1}\right], \quad (15)$$

which is equivalent to Equation 33 of B. T. Draine & A. Li (2001)[3]. The energies resulting from this model are shown in Figure 3 for a range of grain sizes.

We calculate the PAH cross-section following the method described in B. T. Draine et al. (2021) and B. T. Draine et al. (2025).

4. VALIDATION

4.1. *Single Grain Spectra*

In the left panel of Figure 4.1, we present the resulting spectrum for a 5.01 Å ionized grain in the modified Mathis, Mezger, and Panagia (mMMP) radiation field (J. S. Mathis et al. 1983) (described in B. T. Draine 2011) ranging in intensity from $U = 1 - 10^4$. We used a set of 543 basis spectra spanning $0.091 - 20.1$ μm with a spacing of $\Delta\lambda = 0.01$. We compare the analogous spectra from B. T. Draine et al. (2021) (generated using the method described in B. T. Draine & A. Li 2001) by overplotting them for each intensity in the black dotted lines. The bottom panel shows the fractional residuals between models for each intensity.

Overall, the two methods exhibit good ($\sim 10\%$) agreement for all $\log U$ over wavelengths of $\sim 1 - 10$ μm. There is a relatively small U-dependence exhibited in the residuals, with our model reproducing p_λ slightly better for lower intensities. The sharp features in the residuals are a result of small differences in the narrow emission features, caused by a slight disagreement between the $C_{\rm abs}$ values used in B. T. Draine et al. (2021) and our model. Since our $C_{\rm abs}$ are based entirely on the $C_{\rm abs}$ model from B. T. Draine et al. (2021), we believe that these differences are due to an implementation bug and/or interpolation effects, and will not affect our final results.

[3] Note that Equation 10 of B. T. Draine & A. Li (2001), which describes f_2, is mistakenly defined to be a factor of n^2 smaller than the correct definition of f_2, but this mistake was not carried over to their calculations.

The models disagree most significantly at long wavelengths. The source of this disagreement is likely due to differences in the physical approximations made by the models, rather than our model's inability to capture multi-photon heating effects. The specific cause may be due to differences in the low-energy discretization used in the B. T. Draine & A. Li (2001) method and the continuous cooling treatment applied by our model.

The right panel of Figure 4.1 shows the same plot, but for a 15.0 Å ionized grain. For $\log U$ of 0 and 1, our model once again reproduces the B. T. Draine et al. (2021) to very good agreement, particularly at long wavelengths. Multi-photon effects begin to appear at short wavelengths, particularly in the $\log U = 3$ and 4 radiation fields. The 15.0 Å grain's higher absorption cross-section results in the grain spending a higher fraction of its time in higher-energy states. This leads to a higher fraction of near-IR emission, which our model fails to capture. However, the overall near-IR emission from these grains is negligible compared to contributions from smaller grains, so these differences will have little effect on the near-IR portion of the size-integrated spectrum.

4.2. *Size-integrated Spectra*

In Figure 4.2, we show results for ionized PAHs in the mMMP radiation field integrated over the entire grain size distribution (using the size distribution described in B. S. Hensley & B. T. Draine 2023). We once again show results for radiation field intensities ranging from $1 - 10^4$, and overplot the analagous B. T. Draine et al. (2021) models in the black dotted lines. The bottom panel shows the fractional residuals between our model and B. T. Draine et al. (2021) as a function of U.

Overall, a majority of the size-integrated spectra exhibit excellent agreement with the models from B. T. Draine et al. (2021). In particular, the $\log U = 0$ and 1 models agree to within $< 10\%$ of B. T. Draine et al. (2021) across a majority of the JWST wavelength range. The $\log U = 2$, 3, and 4 spectra agree similarly well below roughly 10, 7, and 4 μm, respectively. All models are fairly successful in reproducing the 3.3 μm feature, suggesting that the dominant carriers of this feature remain reliably in the single-photon regime across a wide range of radiation environments.

5. CODE

The methods described in Section 2 have been implemented into a set of Python routines that will be publicly available upon the submission of this paper. The primary functions included in the code are as follows:

```
calc_cabs(wavelength_arr, radius_arr)
```

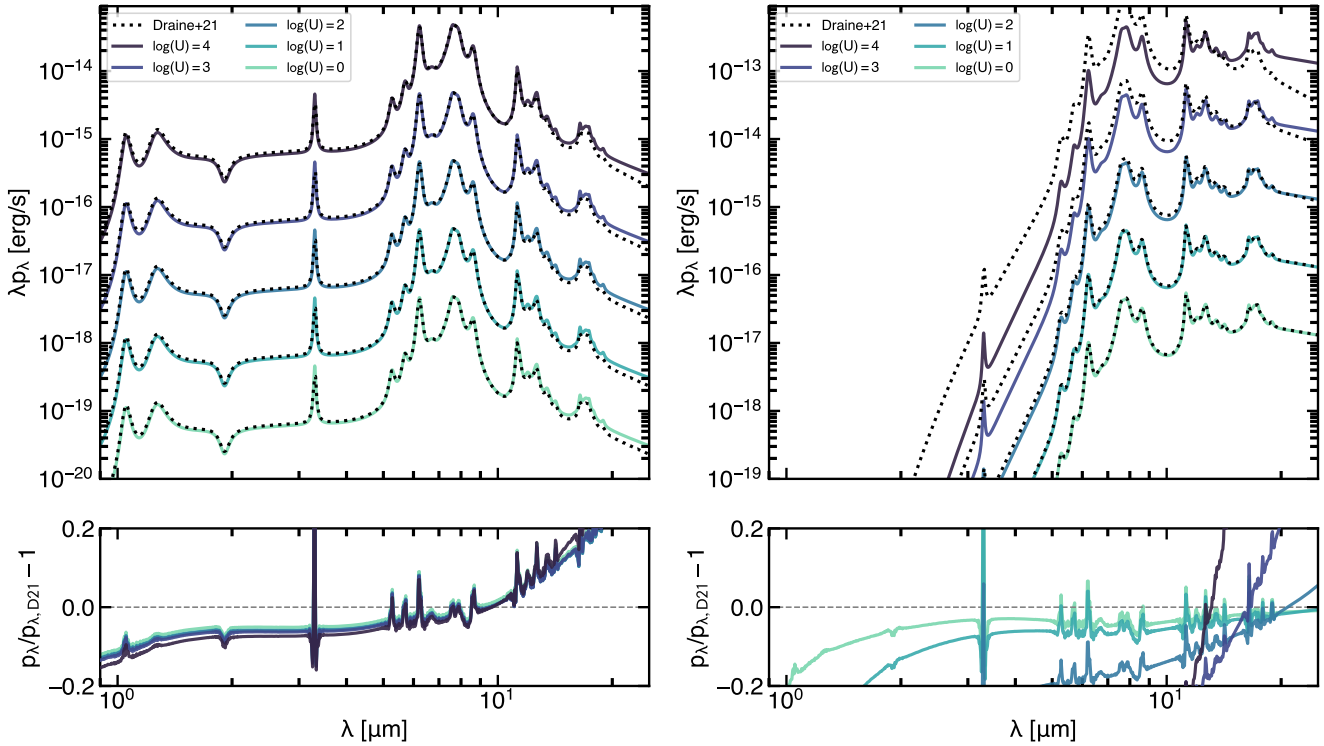

Figure 3. (Top left) the integrated spectra, p_λ, for a 5.01 Å ionized grain in the mMMP radiation field using our model (solid colored lines) and the equivalent spectra from B. T. Draine et al. (2021) (black dotted lines). The line color indicates the radiation field intensity, U, which ranges from $1 - 10^4$. (Bottom left) the fractional residuals between our model and the B. T. Draine et al. (2021) models for each U. (Right) same as the left panel, but for a 15.0 Å ionized grain.

Calculates $C_{\rm abs}$ following the method described in B. T. Draine et al. (2021) and B. T. Draine et al. (2025) for neutral and ionized PAHs for arbitrary wavelengths and grain sizes, assuming $a \ll \lambda$.

```
calc_pah_energy(grain_radius, temp_arr)
```

Calculates the PAH energy function, $E(T)$, for an input temperature range and grain size following the method described in Section 3. Depending on the input effective radius, a, `calc_pah_energy()` calls one of two subroutines: `calc_pah_energy_modes()` for $N_{\rm C}(a) \leq 7360$ (i.e. Equation 11) and `calc_pah_energy_debye()` for $N_{\rm C}(a) > 7360$ (i.e. Equation 15).

```
calc_pah_cooling(lambda_abs, grain_radius,
                 wavelength_arr, c_abs_arr,
                 temp_arr, energy_arr)
```

Solves for the PAH cooling function, $T(t)$, given an input $\lambda_{\rm abs}$ and grain size. The routine does this by first integrating Equation 2 over the input `wavelength_arr` (which must span a wavelength range sufficient to capture the emission wavelength range of PAHs, i.e., $\sim 0.1 - 3000\ \mu m$) to determine dE/dt, assuming that the initial temperature is given by the temperature corresponding to $E_{\rm abs}(T) = hc/\lambda_{\rm abs}$. It then applies this dE/dt to Equation 3, with dt chosen such that dE is 0.001% of the grain's current energy, ensuring that the energy does not change rapidly. The updated grain energy is then used to determine its current temperature, and this loop repeats until the grain has cooled to 5 K.

```
calc_basis_vectors(wavelength_arr,
                   weighting_arr, temp_arr,
                   c_abs_arr)
```

Applies the output $T(t)$ from `calc_pah_cooling()` for a given $\lambda_{\rm abs}$ to Equation 4 to generate $p_{\lambda_{\rm em}}(\lambda_{\rm abs})$. We apply a weighting array to the sum in Equation 4 to account for our use of an adaptive timestep, calculated as `weighting = dt_arr / sum(dt_arr)`.

```
calc_normalization(lambda_abs, dlambda,
                   grain_radius,
                   wavelength_arr,
                   p_lambda_arr,
                   wavelength_arr_u,
                   u_lambda_arr)
```

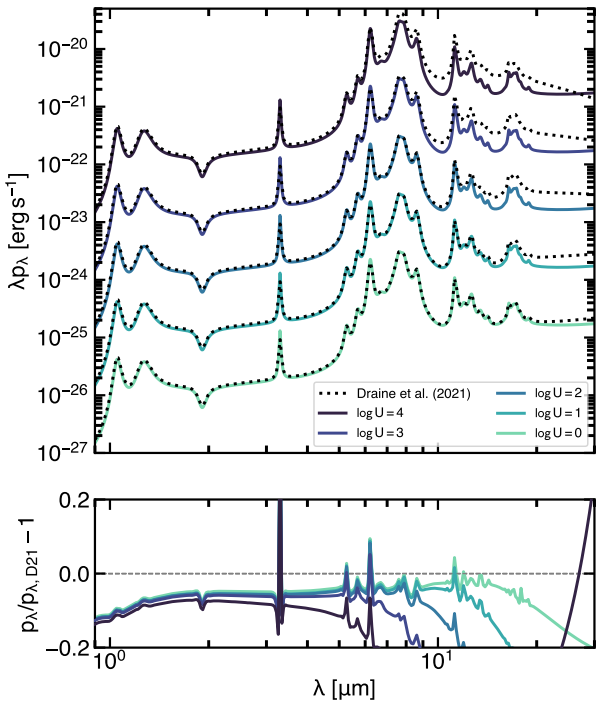

Figure 4. The size-integrated spectrum for ionized grains in the mMMP radiation field.

Applies the normalization in Equation 6 to the input $p_{\lambda_{\rm em}}(\lambda_{\rm abs})$ according to the power of input radiation field, `u_lambda`, over the range `[lambda_abs, lambda_abs * (1 + dlambda)]`.

5.1. *Defining* $\tilde{p}_{\lambda_{\rm em}}(\lambda_{\rm abs})$

Each $\lambda_{\rm abs}$ used in this routine will correspond to its own basis spectrum, $\tilde{p}_{\lambda_{\rm em}}(\lambda_{\rm abs})$. It would be computationally infeasible to generate basis spectra for every relevant photon wavelength. Therefore, we choose to define our $\lambda_{\rm abs}$ wavelengths such that they span the relevant range (i.e., where the energy emitted by u_λ contributes significantly to PAH heating) with a fixed spacing of $\lambda_{\rm abs}\Delta\lambda$ between each $\lambda_{\rm abs}$. Then, the power absorbed from the radiation field "photon" is integrated over a small range, $[\lambda_{\rm abs}, \lambda_{\rm abs}(1+\Delta\lambda)]$. We find that the resulting spectrum is converged for $\Delta\lambda \leq 0.01$. It is crucial that the input $p_{\lambda_{\rm em}}(\lambda_{\rm abs})$ is defined for all $\lambda_{\rm abs}$ where the u_λ array is defined, or at least where the power from u_λ contributes significantly to PAH heating. If they are not, then the integrated spectrum given by Equation 7 will not include energy absorbed from photons at those wavelengths. It is also imperative that the input `dlambda` and `lambda_abs` values are equivalent to those used to generate the input basis spectra. If `dlambda` is larger or smaller than the value used to define the basis spectra, this normalization will either over- or under-count the energy absorbed from the radiation field. We provide a utility function for defining the $\lambda_{\rm abs}$ array, `generate_photon_wavelengths()`.

6. SUMMARY AND OUTLOOK

We developed a new method for generating theoretical PAH emission spectra using the single-photon approximation for PAH heating. So far, this work has consisted of formulating the model described in Section 2 and implementing our method into a Python-based tool, which will be publicly available upon the submission of this paper. We also generated single-grain and size-integrated spectra, which we compared our model spectra to theoretical models that include a full treatment of PAH heating (B. T. Draine & A. Li 2001) from B. T. Draine et al. (2021).

This work has shown that the single-photon approximation for PAH heating and emission can produce excellent ($\lesssim 10\%$) agreement with existing theoretical PAH emission spectra. This method opens up a new avenue for studying the dependence of PAH emission features on the radiation environment in the JWST wavelength range. With the radiation field as a free parameter, it is possible to disentangle degeneracies between the PAH size distribution and ionization fraction and the radiation environment in PAH band ratios. Because scaling the basis spectra to the radiation field is relatively fast, this method enables the exploration of wider ranges of parameter space with MCMC-style fitting.

We plan to publish our model in this paper, along with a Python-based tool and a set of basis spectra that can be used to quickly generate PAH emission spectra for arbitrary input radiation fields. In addition to the current contents of this paper, we will include single-grain and size-integrated spectra for neutral PAHs, along with an investigation of the relationship between grain size, illuminating photon energy, and PAH band ratios for neutral and ionized PAHs. We will also include a method of quantifying the ability of this model to reproduce the full emission spectrum depending on the grain size and radiation field, which depends on the PAH cooling timescale and the radiation field photon absorption timescale. We are still investigating the source of disagreement between ours and the B. T. Draine et al. (2021) absorption cross-sections, which is the cause of the disagreement between the narrow features in the spectra. This is likely due to an implementation error, and will hopefully be resolved by the release of this paper.

ACKNOWLEDGMENTS

This work originated from a project of the Summer Program in Astrophysics 2025 held at the University of

Virginia, and funded by the Center for Global Inquiry and Innovation, the National Science Foundation (Grant 2452494), the National Radio Astronomy Observatory (NRAO), the Kavli Foundation and the Heising-Simons Foundation.

Software: astropy (Astropy Collaboration et al. 2013, 2018, 2022)

REFERENCES

Allamandola, L. J., Tielens, A. G. G. M., & Barker, J. R. 1985, ApJL, 290, L25, doi: 10.1086/184435

Astropy Collaboration, Robitaille, T. P., Tollerud, E. J., et al. 2013, A&A, 558, A33, doi: 10.1051/0004-6361/201322068

Astropy Collaboration, Price-Whelan, A. M., Sipőcz, B. M., et al. 2018, AJ, 156, 123, doi: 10.3847/1538-3881/aabc4f

Astropy Collaboration, Price-Whelan, A. M., Lim, P. L., et al. 2022, ApJ, 935, 167, doi: 10.3847/1538-4357/ac7c74

Baron, D., Sandstrom, K. M., Rosolowsky, E., et al. 2024, ApJ, 968, 24, doi: 10.3847/1538-4357/ad39e5

Baron, D., Sandstrom, K. M., Sutter, J., et al. 2025, ApJ, 978, 135, doi: 10.3847/1538-4357/ad972a

Draine, B. T. 2011, Physics of the Interstellar and Intergalactic Medium

Draine, B. T., & Li, A. 2001, ApJ, 551, 807, doi: 10.1086/320227

Draine, B. T., Li, A., Hensley, B. S., et al. 2021, ApJ, 917, 3, doi: 10.3847/1538-4357/abff51

Draine, B. T., Li, A., Hensley, B. S., et al. 2025, ApJ, 989, 232, doi: 10.3847/1538-4357/adf737

Hensley, B. S., & Draine, B. T. 2023, ApJ, 948, 55, doi: 10.3847/1538-4357/acc4c2

Leger, A., & Puget, J. L. 1984, A&A, 137, L5

Li, A. 2020, Nature Astronomy, 4, 339, doi: 10.1038/s41550-020-1051-1

Mathis, J. S., Mezger, P. G., & Panagia, N. 1983, A&A, 128, 212

Tielens, A. G. G. M. 2008, ARA&A, 46, 289, doi: 10.1146/annurev.astro.46.060407.145211